Talanta 117 (2013) 338–344

Contents lists available at ScienceDirect

Talanta

journal homepage: www.elsevier.com/locate/talanta

A highly sensitive and selective turn-on fluorogenic and colorimetric sensor based on pyrene-functionalized magnetic nanoparticles for Hg^{2+} detection and cell imaging

Ling Chen [a], Baozhan Zheng [a], Yong Guo [a], Juan Du [a,*], Dan Xiao [a,b,**], Lin Bo [c]

[a] College of Chemistry, Sichuan University, No. 29 Wangjiang Road, Chengdu 610064, PR China
[b] College of Chemical Engineering, Sichuan University, 29 Wangjiang Road, Chengdu 610064, PR China
[c] Regenerative Medicine Research Center, West China Hospital, Sichuan University, 4 Keyuan Road, Chengdu 610041, China

ARTICLE INFO

Article history:
Received 19 April 2013
Received in revised form
1 September 2013
Accepted 2 September 2013
Available online 7 September 2013

Keywords:
Fluorescent sensor
Py–Si–Fe_3O_4@SiO_2 NPs
Magnetic core/shell
Water samples and serum sample
Hg^{2+}
Living cells

ABSTRACT

In this paper, a colorimetric and "turn-on" fluorescent sensor (Py–Si–Fe_3O_4@SiO_2 NPs) for Hg^{2+} detection was designed with pyrene derivative covalently grafted onto the surface of magnetic core/shell Fe_3O_4@SiO_2 nanoparticles using the silanol hydrolysis approach. The Py–Si–Fe_3O_4@SiO_2 inorganic–organic hybrid material was characterized by scanning electron microscopy (SEM), transmission electron microscopy (TEM), X-ray power diffraction (XRD), Fourier transform infrared spectroscopy (FTIR), and fluorescence emission. The results of fluorescence spectra showed that the resultant multifunctional nanoparticles exhibited selective turn-on type fluorescence enhancement with Hg^{2+}. In addition, the presence of magnetic Fe_3O_4 nanoparticles in the sensor Py–Si–Fe_3O_4@SiO_2 NPs would also facilitate the magnetic separation of Hg^{2+}–Py–Si–Fe_3O_4@SiO_2 from the solution. The as-prepared chemosensor was also successfully applied to detect Hg^{2+} in environmental water samples and serum sample. Results from confocal laser scanning microscopy experiments demonstrated that this chemosensor was cell permeable and can be used as a fluorescent probe for monitoring Hg^{2+} in living cells.

1. Introduction

Heavy metal pollution is widespread and arises from a variety of industrial sources [1,2]. Hg^{2+} is considered to be one of the most common and toxic metal ions that are being investigated for recognition studies. The extreme toxicity of mercury and its derivatives results from their affinities toward thiol groups in proteins and enzymes [3,4]. More importantly, the Hg^{2+} ion present in soil or effluent water is assimilated by the lower aquatic organisms, which are known to convert it to methylmercury, one of the most potent neurotoxins for human race [5–7]. Hg^{2+} is a heavy metal ion that is recognized as a fluorescence quencher due to the enhancement of spin–orbit coupling commonly associated with the heavy atom effect [8,9]. In terms of sensitivity concerns, chemosensors exhibiting fluorescence enhancement (fluorescence "turn-on") upon Hg^{2+} complexation are favoured over those showing fluorescence quenching (fluorescence"turn-off") under Hg^{2+} binding. Moreover, fluorescence "turn-off"probes may report false positive results caused by other quenchers in practical samples and are undesirable for practical analytical applications. Therefore, it would be advantageous to design fluorescent sensors that can turn on fluorescence and provide a specific response following Hg^{2+} recognition [10–12].

Magnetic microspheres consisting of a magnetically responsive core and a silica shell have gathered a lot of attention. Firstly, the magnetically responsive core makes it easy to isolate and recycle quickly from matrix solutions via external magnetic field. Secondly, they also have advantages for the design of biological fluorescent probes because of their low toxicity and biocompatibility. Furthermore, the silica shell around magnetic core has large surface area, and it can be grafted by fluorescent probes [13]. It is known that most of the fluorescence could be quenched if a fluorescent dye is attached on the surface of iron oxide nanoparticles. But if the dye is far away enough from the core iron oxide, quenching of the fluorescence will be prevented [14]. Therefore, the thick silica layer would be used as the support of fluorescent probes, and also to keep the distance between the core and the surface. Thus, with small molecular fluorescent probes incorporated, magnetic silica nanoparticle is a desirable material to develop nontoxic, biocompatible, and recoverable fluoremetric Hg^{2+} sensors.

In our work, an inorganic–organic hybrid nanomaterial has been prepared by immobilizing pyrene derivative onto the surface of

* Corresponding author.
** Corresponding author at: College of Chemistry, Sichuan University, No. 29, Wangjiang Road, Chengdu 610064, PR China. Tel.: +86 28 85416029; fax: +86 28 85415029.
E-mail address: xiaodan@scu.edu.cn (D. Xiao).

0039-9140/$ - see front matter © 2013 Elsevier B.V. All rights reserved.
http://dx.doi.org/10.1016/j.talanta.2013.09.001

Fe_3O_4@SiO_2 magnetic silica nanocomposite. This colorimetric and "turn-on" fluorescent chemosensor (Py–Si–Fe_3O_4@SiO_2) shows high performance in the detection of Hg^{2+} with a detection limit of 11 ng/mL. Furthermore, Py–Si–Fe_3O_4@SiO_2 can quickly separate Hg^{2+} from the solution with external magnetic field. The Py–Si–Fe_3O_4@SiO_2 is employed as Hg^{2+} sensor in water samples and serum sample. It is also applied for living cells imaging.

2. Experimental

2.1. Apparatus

^{1}H NMR spectra were recorded on Varian Inova 400 MHz. ^{13}C NMR spectra were recorded on Bruker AV II-400 MHz. Mass spectra were obtained with an ion trap mass spectrometer (LCQ Fleet; Thermo Fisher Scientific, San Jose, CA). The crystal structures of Fe_3O_4@SiO_2, OCN-Fe_3O_4@SiO_2, and Py–Si–Fe_3O_4@SiO_2 were analyzed by a Tongda TD-3500 X-ray powder diffractometer (Liaoning, China) with Cu-Ka radiation (λ=0.15148 nm) operating at 30.0 kV and 20.0 mA. Fourier transform infrared spectra (FT-IR) were recorded on a Thermo Scientific Nicolet 6700 FT-IR spectrometer (Sugar Land, TX, USA). Scanning electronic microscopy (SEM) images were recorded on a JSM-7500 F. Transmission electron microscopy (TEM) images were taken with a Hitachi-H800 transmission electron microscope (Tokyo, Japan). Fluorescence spectra were measured on a Hitachi F-7000 spectrophotometer equipped with a 1 cm quartz cell.

2.2. Reagents

1-Pyrenecarboxaldehyde (99%) was purchased from Alfa Aesar; 3-(Triethoxysilyl)-propyl isocyanate (TESPIC) (96%) was purchased from J&K. Hydrazine hydrate (50%) was provided by Kemiou (Tianjin); All solvents were redistilled before use. All other chemicals were of analytical-reagent grade and were used without further purification.

2.3. Synthesis of TESPIC-modified silica particles (denoted as OCN-Fe_3O_4@SiO_2 core–shell NPs)

2.3.1. Preparation of Fe_3O_4 NPs

In this paper, Fe_3O_4 NPs were synthesized through a similar way with Morel [15]. A freshly prepared mixture of 0.750 mmol $FeCl_3 \cdot 6\,H_2O$ and 0.375 mmol $FeCl_2 \cdot 4H_2O$ in 5.00 mL of 0.05 M HCl was rapidly injected to 40.0 mL of 2 M ammonia solution containing 0.01 M of hydrazine under power ultrasound at room temperature in an nitrogen flow. The mixture was sonicated for 1 h. The sediment was separated with a permanent magnet, and washed three times with 0.1 M NaCl solution and distilled water. The precipitate was dispersed in 10.0 mL distilled water.

2.3.2. Preparation of Fe_3O_4@SiO_2 core–shell NPs

Fe_3O_4@SiO_2 core–shell NPs were synthesized according to the study of Stjerndahl et al. [16]. Then, the Fe_3O_4@SiO_2 core–shell NPs were synthesized as follows: First, water (450 μL) and aqueous ferrofluid (900 μL) were mixed by sonication and added to an organic surfactant solution of cyclohexane (22.5 mL), Triton X-100 (5.31 mL), and 1-hexanol (5.40 mL) to form a w/o microemulsion. Next, tetraethoxysilane (TEOS) (100 μL) and ammonium hydroxide (100 μL) were added, and the sample was mechanically stirred for one day at room temperature. To separate the particles, ethanol was added to break the microemulsion. The resulting nanocomposites were separated with a permanent magnet, and washed with ethanol and water (2 × ethanol, 2 × water) and then dried in vacuum at 40 °C overnight.

2.3.3. Preparation of OCN-Fe_3O_4@SiO_2 core–shell NPs

Fe_3O_4@SiO_2 core–shell NPs were dispersed in anhydrous toluene (50.0 mL) and then 3-(Triethoxysilyl)-propyl isocyanate (TESPIC) (0.280 mL, 0.940 mmol) was added. The sample was mechanically stirred for 12 h at room temperature. The resulting nanocomposites were separated with a permanent magnet, and washed several times with toluene.

2.4. Synthesis of compound Py-Schiff base

To a solution of 1-pyrenecarboxaldehyde (2 mmol) in ethanol (25.0 mL), 5.00 mL (excess) hydrazine hydrate (50%) was added. The solution was refluxed for 5 h and then allowed to stand at room temperature overnight. The precipitate was filtered, washed thoroughly with ethanol and dried under reduced pressure to afford compound Py-Schiff base (90%) as a yellowish crystal.

^{1}H NMR (400 MHz, CD_3COCD_3) δ (ppm): 2.92 (s, 2H, NH), 8.11 (t, J=8.0 Hz, 1H, ArH), 8.24–8.19 (m, 2H, ArH), 8.35–8.31 (m, 4H, ArH), 8.65 (d, J=8.0 Hz, 1H, ArH), 9.10 (d, J=8.0 Hz, 1H, ArH), 9.31 (s, 1H, CH=N) (Fig. S1). ^{13}C NMR (400 MHz, CD_3COCD_3) δ (ppm): 124.2, 125.3, 125.7, 125.9, 126.7, 127.0, 127.3, 127.6, 128.3, 128.5, 129.6, 129.7, 130.7, 31.6, 132.3, 133.8 (Fig. S2). ESI-MS m/z: $[M+H]^+$ calcd for $C_{17}H_{12}N_2$: 245.3; found, 245.2 (Fig. S3).

2.5. Synthesis of pyrene-functionalized magnetic silica nanocomposites (Py–Si–Fe_3O_4@SiO_2 NPs)

Py–Si–Fe_3O_4@SiO_2 was synthesized according to the reported method [17]. Py-Schiff base and OCN-Fe_3O_4@SiO_2 core–shell NPs were suspended in anhydrous toluene (50.0 mL) and stirred under reflux in N_2 atmosphere for 48 h. The resulting nanocomposites were washed several times with toluene and acetone by centrifugation.

2.6. Cell Incubating

The living HUVEC cells were provided by Regenerative Medicine Research Center, West China Hospital, Sichuan University (Sichuan, China). Confocal fluorescence imaging was performed with a Nikon A1 laser scanning confocal microscope (excitation wavelength 405 nm). The HUVEC cells were incubated with high glucose medium (H-DMEM) (Gibco, USA) supplemented with 10% fetal calf serum (FBS) (Gibco, USA) for three days at 37 °C. Then the HUVEC cells were incubated with 0.15 g/L solution of Py–Si–Fe_3O_4@SiO_2 for 1 h at 37 °C. After renewing the medium, the HUVEC cells were incubated with 25 μM $Hg(NO_3)_2$ for another 5 h at 37 °C. Following incubation, the cells were imaged.

3. Results and discussion

3.1. Synthesis and characterization of Py–Si–Fe_3O_4@SiO_2

The synthetic protocol is represented in Scheme 1. The structure of Py-Schiff base was confirmed by MS data and ^{1}H NMR and ^{13}C NMR spectra. The morphology of Py–Si–Fe_3O_4@SiO_2 was examined by SEM (Fig. 1) and TEM (inset of Fig. 1). As revealed by SEM images, the obtained Py–Si–Fe_3O_4@SiO_2 particles have an average diameter of 143 nm with a spherical shape (Fig. S5). It also shows that some of the NPs are aggregated because of the magnetic dipolar interaction among the magnetite NPs. From Fig. 1 inset the coated silica layer as the typical core–shell structure of Py–Si–Fe_3O_4@SiO_2 can be observed, black spots showing Fe_3O_4 and ash part as SiO_2 shell. This indicates the successful synthesis of magnetic core/shell particles. The inset of Fig. 1 reveals that the prepared NPs have shell thicknesses of about 60 nm, whereas the SEM image proves that these core–shell magnetic silica microspheres have an even surface

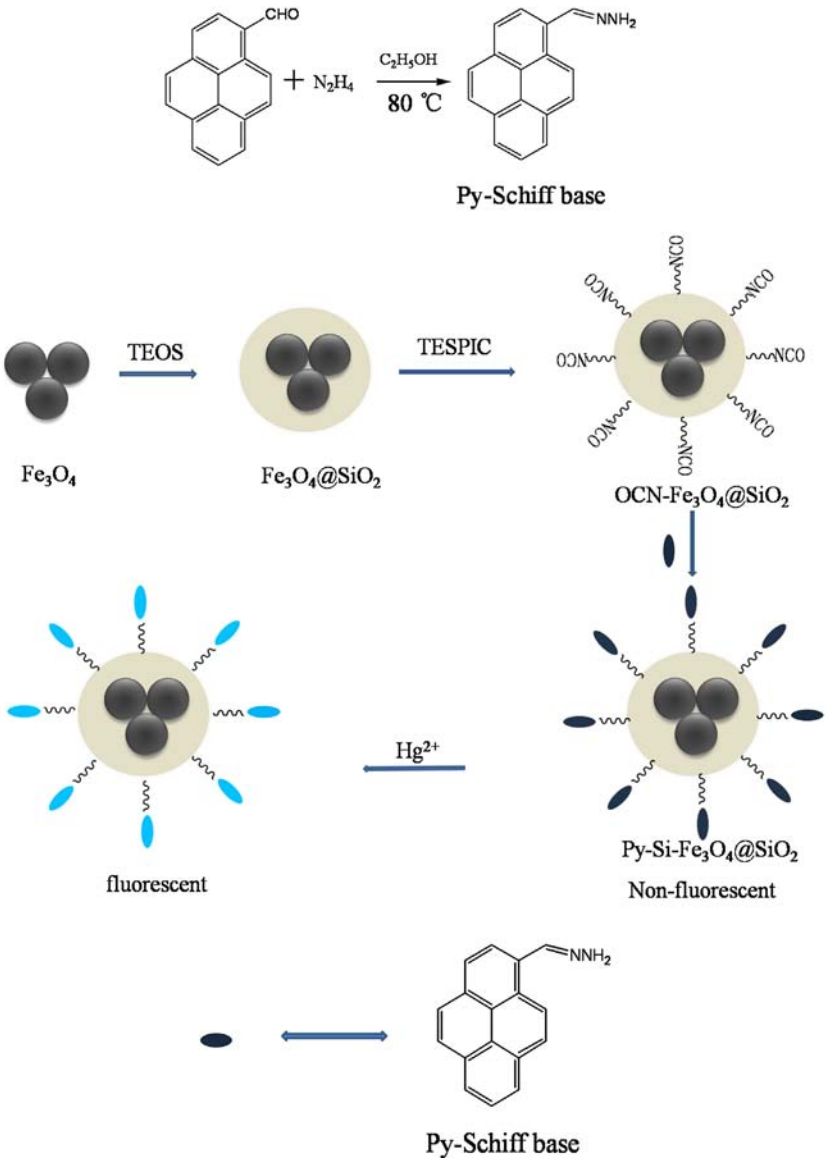

Scheme 1. Synthesis Procedure for the Functionalized Material Py–Si–$Fe_3O_4@SiO_2$. .

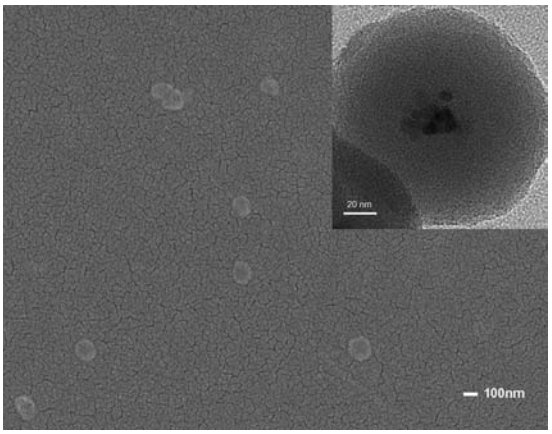

Fig. 1. SEM image of Py–Si–$Fe_3O_4@SiO_2$ microspheres. Inset: TEM image of Py–Si–$Fe_3O_4@SiO_2$ microspheres.

morphology, which endows them with both the special surface property and the large external surface area that is desirable for molecular immobilization.

Fig. 2 shows the XRD patterns of $Fe_3O_4@SiO_2$, OCN-$Fe_3O_4@SiO_2$, and Py–Si–$Fe_3O_4@SiO_2$ respectively. The six characteristic diffraction peaks in Fig. 3 can be indexed to (220), (311), (400), (422), (511), and (440), which are well agree with the database of magnetite in the Joint Committee on Powder Diffraction Standards [JCPDS] (JCPDS card: 19-629) file [13]. However, the characteristic diffraction peaks of Fe_3O_4 are weakened because of the solid silica coat, and the Py-Schiff base-modification. Meanwhile, a broad diffraction peak centered around 22° of 2θ is assigned to amorphous silica [18,19].

The FTIR spectra of OCN-$Fe_3O_4@SiO_2$, Py–Si–$Fe_3O_4@SiO_2$, and Py-Schiff base are shown in Fig. 3. The strong broad band at around 1091 cm^{-1} corresponds to the Si–O–Si asymmetric stretching vibration. The weak band found at 2312 cm^{-1} is assigned to isocyanates region [20]. The band at 3359 cm^{-1} is assigned to the N–H stretching vibrational mode [21]. The band at 3040 cm^{-1} is due to the aromatic C–H stretching vibration [22]. The band located at 1689 cm^{-1} is assigned to the carbonyl stretching vibration of the amides [23–25]. The 1591 cm^{-1} peak is due to a ring stretching mode of aromatic group [26]. These results suggest that Py-Schiff base has been successfully loaded on the self-prepared OCN-$Fe_3O_4@SiO_2$ magnetic nanoparticles.

Fig. 4 shows photographs of the dispersion and redispersion of Py–Si–Fe_3O_4@SiO_2 under an external magnetic force. As shown in Fig. 4a, the Py–Si–Fe_3O_4@SiO_2 microspheres can be uniformly dispersed in solution by vigorous shaking or sonication, resulting in a stable black suspension. When a magnet was set close to the glass vial containing the magnetic NPs, the NPs were attracted toward the magnet very quickly and accumulated to the side of the glass vial near the magnet within one minute, resulting in a clear and transparent yellow solution (Fig. 4b). Redispersion occurred quickly with a slight shaking once the magnetic field was removed (Fig. 4c). Thus, the attraction and dispersion processes can be readily altered by applying and removing an external magnetic field, showing good dispersion and magnetic separation. These results show that Py–Si–Fe_3O_4@SiO_2 microspheres possess excellent magnetic responsivity and redispersibility, which is important in terms of their practical manipulation. The magnetic separation capability of Py–Si–Fe_3O_4@SiO_2 in this detection method can also offer a simple and efficient route to separate Hg^{2+} from various environments.

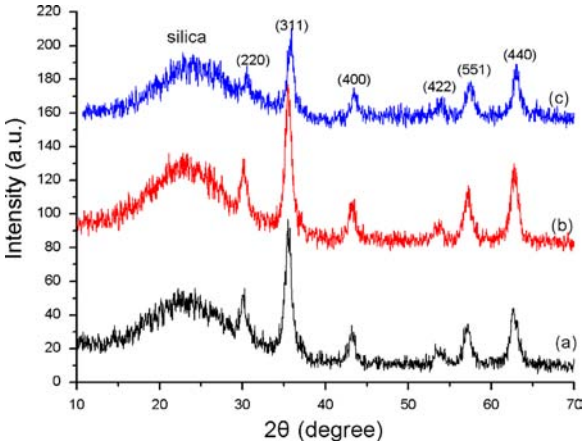

Fig. 2. The wide-angle XRD patterns of (a) Fe_3O_4@SiO_2, (b) OCN-Fe_3O_4@SiO_2, and (c) Py–Si–Fe_3O_4@SiO_2.

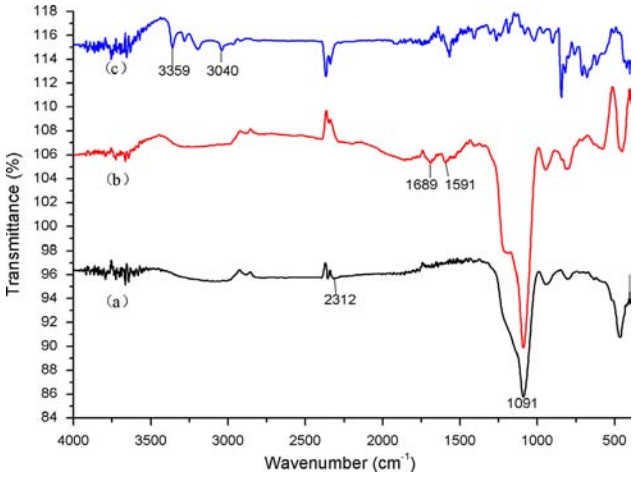

Fig. 3. The FT-IR spectra of (a) OCN-Fe_3O_4@SiO_2, (b) Py–Si–Fe_3O_4@SiO_2 and (c) Py-Schiff base.

3.2. *Sensing performance of the Py–Si–Fe_3O_4@SiO_2 toward Hg^{2+}*

Fig. S4 shows the impact of the ratio of acetone and water content on the fluorescence intensity of Py–Si–Fe_3O_4@SiO_2. The fluorescence intensity first increases with increasing acetone content, and reaches its maximum when $V_{acetone}/V_{total}=3/4$, then with the further increasing of acetone content, the fluorescence intensity begins to decrease. In order to get excellent spectroscopic properties and relatively good water solubility at the same time, the following experiments were all carried out in acetone/water (3:1, v/v) (Fig. S4). Upon addition of Hg^{2+}, the solution color of Py–Si–Fe_3O_4@SiO_2 (0.4 g/L) correspondingly changed from yellow to colorless (Fig. 5a). Using hand-held UV light irradiation, Py–Si–Fe_3O_4@SiO_2 alone exhibited almost no fluorescence, the addition of 10 μM Hg^{2+} resulted in a prominent enhancement of blue-fluorescence (Fig. 5b). These results demonstrated that the Py–Si–Fe_3O_4@SiO_2 NPs can act as a useful colorimetric and fluorogenic sensor for Hg^{2+} detection.

Selectivity is a very important parameter to evaluate the performance of a fluorescence chemosensor. The interference of a number of common metal ions, including K^+, Ca^{2+}, Ba^{2+}, Mg^{2+}, Zn^{2+}, Mn^{2+}, Ni^{2+}, Cd^{2+}, Pb^{2+}, and Cu^{2+}, for detection of Hg^{2+} with Py–Si–Fe_3O_4@SiO_2 (0.4 g/L) was carried out with excitation fixed at 363 nm and emission at 450 nm. Fig. 6a illustrates the fluorescence responses of Py–Si–Fe_3O_4@SiO_2 to different metal ions of interest. Upon addition of 50 μM of Hg^{2+}, the fluorescence intensity of Py–Si–Fe_3O_4@SiO_2 underwent a dramatic increase. As for the other metal ions, only Pb^{2+} and Cu^{2+} promoted small fluorescence intensity change. To test the practical applicability of our fluorescent chemosensor for Hg^{2+}, competition experiments were also carried out by adding another 1 equivalent of various of other metal ions to the solution of Py–Si–Fe_3O_4@SiO_2 containing 50 μM Hg^{2+}, respectively, as shown in Fig. 6b. The fluorescence intensity of the solution showed small changes in the presence of other cations. The results in Fig. 6 indicated that our proposed chemosensor was sensitive and selective to Hg^{2+}.

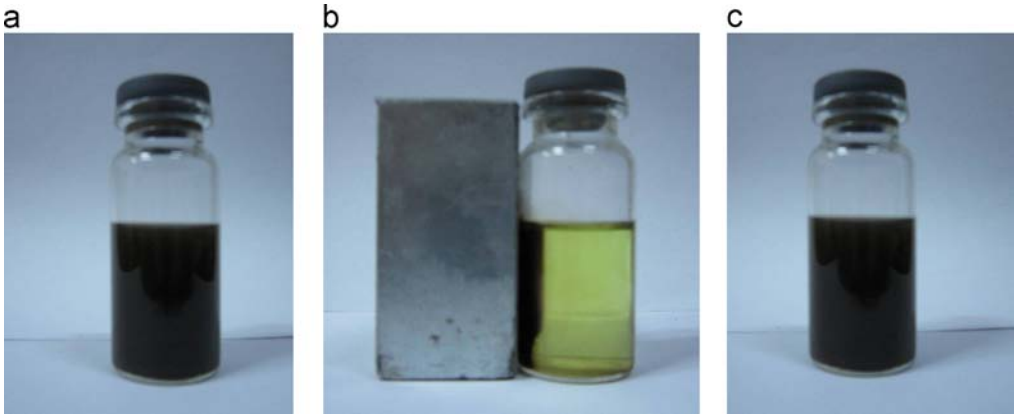

Fig. 4. Photographs of the separation and dispersion processes Py–Si–Fe_3O_4@SiO_2 microspheres: (a) without external magnetic field and (b) with external magnetic field (c) after removing the magnet and slightly shaking.

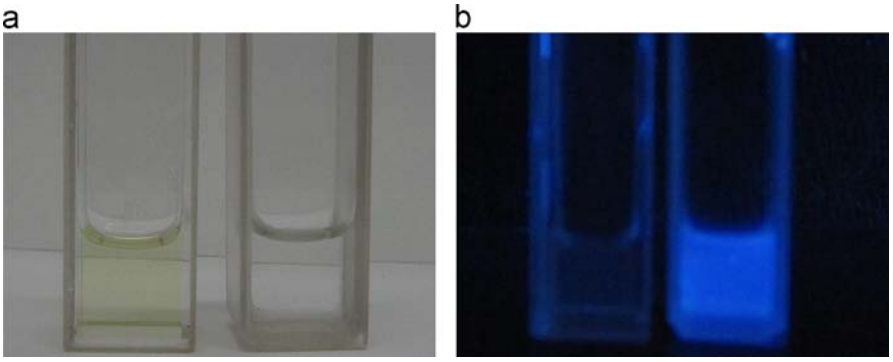

Fig. 5. (a) Photograph of color change of Py–Si–Fe_3O_4@SiO_2 in the absence (left) and presence (right) of 10 μM Hg^{2+} (b) photograph of fluorescence response of Py–Si–Fe_3O_4@SiO_2 in the absence (left) and presence (right) of 10 μM Hg^{2+}.The excitation wavelength was 365 nm.

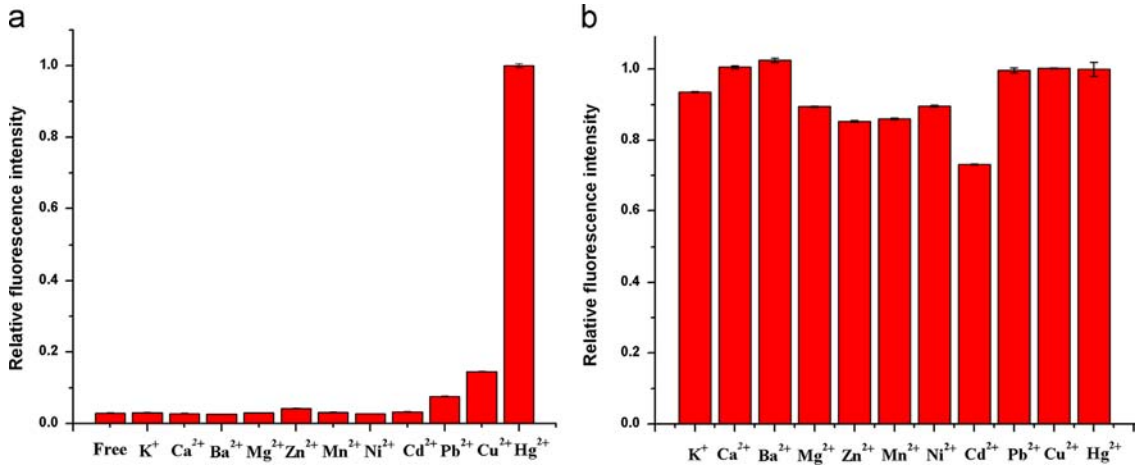

Fig. 6. Fluorescence response of Py–Si–Fe_3O_4@SiO_2 to various cations in ACETONE/WATER (3:1) aqueous solution; (a) the emission intensities of Py–Si–Fe_3O_4@SiO_2 in the presence of various interfering ions (all at 50 μM). (b) The change of the emission that occurs upon the subsequent addition of 1 equivalent of various cations to 50 μM Hg^{2+}.

Py–Si–Fe_3O_4@SiO_2 nanoparticles exhibited very weak fluorescence intensity in solution when excited at 363 nm. The emission spectrum showed typical bands at 386 and 410 nm (Fig. S6a) attributed to the pyrene monomeric emission [27], and a red-shifted maximum at 450 nm (Fig. S6b), which are typical of pyrene excimer fluorescence with low quantum yield [28–31]. The low quantum yield of the Py–Si–Fe_3O_4@SiO_2 resulted from the quenching of the pyrene emission by the lone pair of the nitrogen atom [32] in the free state. So, it could be expected that, upon complexation with a metal cation, the lone pairs no longer participate in the quenching process, causing the recovery of the fluorescence. To evaluate the sensing behavior of Py–Si–Fe_3O_4@SiO_2 toward Hg^{2+}, various concentrations of Hg^{2+} (0–100 μM) were added separately into the solution of Py–Si–Fe_3O_4@SiO_2, as shown in Fig. 7. Upon addition of increasing concentrations of Hg^{2+}, the fluorescence intensity in the 450 nm showed a linear enhancement. With the coordination of Hg^{2+} up to Py–Si–Fe_3O_4@SiO_2, a 58-fold fluorescence enhancement was observed. Meanwhile, the maximum emission wavelength underwent a slight red shift from 445 to 450 nm (Fig. 7). The sensor exhibited a linear response toward Hg^{2+} at the concentration range from 4 μM to 40 μM, the linear equation is $y=kx+b$ ($k=63.19\pm1.87$; $b=-69.66\pm40.48$) and the linear relative coefficient is $R^2=0.994$. The detection limit for the sensor was calculated to be 11.0 ± 0.3 ng/mL according to the 3σ-rule (where σ is the standard deviation of blank solution and $n=10$).

With the purpose of illustrating practical applicability of the proposed method, the probe was applied in the determination of Hg^{2+} in both tap and pond water samples. The water samples were both pretreated with filtration before further determination. All these water samples were spiked with standard Hg^{2+} solutions and then analyzed with proposed probe. The recovery study of

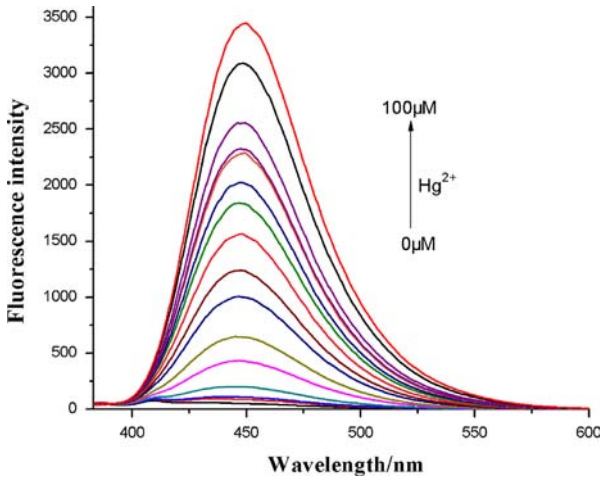

Fig. 7. Fluorescence spectra of Py–Si–Fe_3O_4@SiO_2 upon addition of various amounts of Hg^{2+} ion ($0-1\times10^{-4}$ M) ($\lambda_{ex}=363$ nm) in ACETONE/WATER (3:1) aqueous solution.

spiked Hg^{2+} determined by the sensor shows a satisfactory result (Table 1). Thus, the present probe seems useful for the determination of Hg^{2+} in real samples.

To further demonstrate the applicability of the probe in analysis, the developed sensor was applied to determine the Hg^{2+} in 25-fold diluted serum sample. The serum was purchased from Sichuan University Hospital without further processing. The analytical results were shown in Table 2. These results clearly

indicated that the developed chemosensor was stable in serum sample and can detect Hg^{2+} in the complex serum matrix.

In order to investigate the ability of biological application of Py–Si–Fe_3O_4@SiO_2, the fluorescence imaging experiment was carried out using HUVEC cells. Cultured HUVEC cells were incubated with 0.15 g/L solution of Py–Si–Fe_3O_4@SiO_2 for 1h at 37 °C, and an insignificant amount of Py–Si–Fe_3O_4@Si_2O fluorescence was detected in the cells' interior (Fig. 8a). However, when the cells were supplemented with 25 μM Hg^{2+} for another 5 h at 37 °C, an obvious fluorescence from the intracellular area was observed (Fig. 8b). Bright-field measurements after treatment with Py–Si–Fe_3O_4@SiO_2 and Hg^{2+} confirmed that the cells were viable throughout the imaging experiments (Fig. 8c). The overlay of fluorescence and bright-field images revealed that the fluorescence signals were localized in the perinuclear region of the cytosol (Fig. 8d), indicating the subcellular distribution of Py–Si–Fe_3O_4@SiO_2. These results demonstrated that Py–Si–Fe_3O_4@SiO_2 nanoparticals could be used for monitoring Hg^{2+} with excellent cell-permeability and biocompatibility in living cells.

Comparison of the present probe with other existing Hg^{2+} sensitive turn-on fluorescent probes was presented in Table 3 [33–44]. The results showed the detection limit and the application of our present sensor were comparable and even better than those of other sensors.

Table 1
Results of the Determination of Mercury ion in pond and tap water and the Recovery Test (n=3).

Sample	Added (μM)	Proposed method found (μM)	Recovery (%)	R.S.D. (%)
Tap water	6	5.89 6.16 6.07	98 103 101	2.28
Pond water	8	7.75 8.17 8.03	97 102 100	2.67

Table 2
Recoveries of Mercury ion from spiked serum sample (n=3).

Sample	Added (μM)	Proposed method found (μM)	Recovery (%)	R.S.D. (%)
Serum sample	25	24.5 24.4 24.5	98.0 97.6 98.0	0.236

4. Conclusion

In summary, we have designed and synthesized a pyrene functional core–shell structured magnetic silica nanomaterial as a novel fluorescent chemosensor for detecting Hg^{2+}. It exhibited a fluorescence response toward Hg^{2+} in acetone-water (3:1, v/v) solution with high sensitivity and selectivity. Most importantly, both the colorimetric and fluorescence changes of the chemosensor are remarkably specific for Hg^{2+} in the presence of other heavy and transition metal ions, which meet the selective requirements for biomedical and environmental monitoring application. The

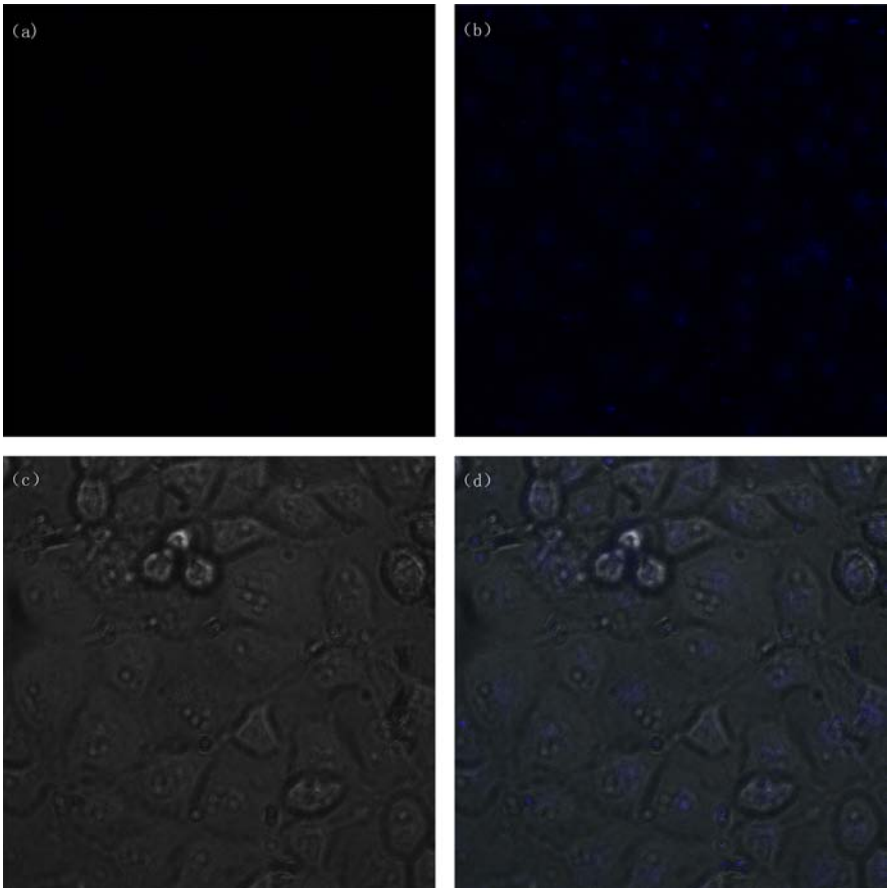

Fig. 8. (a) Fluorescence image of HUVEC cells incubated with 0.15 g/L Py–Si–Fe_3O_4@SiO_2 for 1 h. (b) Confocal image of HUVEC cells that were further incubated with 25 μM Hg^{2+} for another 5 h. (c) Bright field microscopic images of the cells shown in (b). (d) The overlaid image of (b) and (c). The excitation wavelength was 405 nm.

Table 3
Comparison of the present method with the reported fluorescence sensors for the detection of Hg^{2+} in the literature.

Type of sensor	Medium	Detection limit	Application	Reference
Turn-on	$CHCl_3$	15 μM	–	33
Ratiometric	DMSO/aqeuous=9:1	4.3 μM	–	34
Turn-on	CH_3CN/HEPES buffer=3:2	53.6 μM	Living cells imaging	35
Ratiometric	H_2O/DMF=98:2	57.2 nM	–	36
Ratiometric	Water	100 nM	–	37
Turn-on	MeOH/$CHCl_3$=9:1	200 nM	–	38
Turn-on	Water	200 nM	–	39
Turn-off	Water	210 nM	–	40
Turn-on	Acetonitrile/water=9:1	226 nM	Living cells imaging	41
Ratiometric	Water	500 nM	–	42
Turn-on	THF/H_2O=9.5:0.5	2.6 μM	Living cells imaging	43
Turn-on	Acetonitrile	80 nM	Living cells imaging	44
Turn-on	Acetone/water=3:1	55 nM	Pond water and tap water, Blood serum, Living cells imaging	Present work

fluorescence intensity was significantly increased about 58-fold with 100 μM Hg^{2+} added. Furthermore, we have demonstrated that Py–Si–Fe_3O_4@SiO_2 was applicable for Hg^{2+} detection in water samples and serum sample. Besides, the excellent biological value of our magnetic silica nanomaterial was proved by the fluorescence imaging with HUVEC cells. Because of the superparamagnetic core (Fe_3O_4), Py–Si–Fe_3O_4@SiO_2 can also offer a simple and efficient route to separate Hg^{2+} from various environments. We believe that the combination of well-defined inorganic nanomaterials and organic receptors can play a vital role in the development of a new generation of toxic metal ions chemosensor and absorbent.

Acknowledgments

We would express our sincere thanks to the financial support from the National Natural Science Foundation of China (Grant nos. 21177090 and 21075083) and Doctoral Program Foundation of Institutions of Higher Education of China (20120181120075) is gratefully acknowledged. We would like to express our sincere thanks to Analytical & Testing Centre of Sichuan University for the TEM, SEM and NMR measurements.

Appendix A. supplementary material

Supplementary data associated with this article can be found in the online version at http://dx.doi.org/10.1016/j.talanta.2013.09.001.

References

[1] A. Renzoni, F. Zino, E. Franchi, Environ. Res. 77 (1998) 68–72.
[2] J. Benoit, W. Fitzgerald, A. Damman, Environ. Res. 78 (1998) 118–133.
[3] M.M. Pires, J. Chmielewski, Org. Lett. 10 (2008) 837–840.
[4] G.K. Balendiran, R. Dabur, D. Fraser, Cell Biochem. Funct. 22 (2004) 343–352.
[5] P. Mahato, A. Ghosh, S. Saha, S. Mishra, S.K. Mishra, A. Das, Inorg. Chem. 49 (2010) 11485–11492.
[6] Q. Wang, D. Kim, D.D. Dionysiou, G.A. Sorial, D. Timberlake, Environ. Pollut. 131 (2004) 323–336.
[7] H.H. Harris, I.J. Pickering, G.N. George, Science 301 (2003), p. 1203.
[8] H. Masuhara, H. Shioyama, T. Saito, K. Hamada, S. Yasoshima, N. Mataga, J. Phys. Chem. 88 (1984) 5868–5873.
[9] P. Svejda, A.H. Maki, R.R. Anderson, J. Am. Chem. Soc. 100 (1978) 7138–7145.
[10] Y. Zhou, C.Y. Zhu, X.S. Gao, X.Y. You, C. Yao, Org. Lett. 12 (2010) 2566–2569.
[11] S. Voutsadaki, G.K. Tsikalas, E. Klontzas, G.E. Froudakis, H.E. Katerinopoulos, Chem. Commun. 46 (2010) 3292–3294.
[12] J. Fan, K. Guo, X. Peng, J. Du, J. Wang, S. Sun, H. Li, Sensor Actuat. B-Chem. 142 (2009) 191–196.
[13] Y. Wang, X. Peng, J. Shi, X. Tang, J. Jiang, W. Liu, Nanoscale. Res. Lett. 7 (2012) 86.
[14] R. Weissleder, K. Kelly, E.Y. Sun, T. Shtatland, L. Josephson, Nat. Biotechnol. 23 (2005) 1418–1423.
[15] A.-L. Morel, S.I. Nikitenko, K. Gionnet, A. Wattiaux, J. Lai-Kee-Him, C. Labrugere, B. Chevalier, G. Deleris, C. Petibois, A. Brisson, M. Simonoff, ACS Nano 2 (2008) 847–856.
[16] M. Stjerndahl, M. Andersson, E. Holly, D.M. Pajerowski, M.W. Meisel, R.S. Duran, Langmuir 24 (2008) 3532–3536.
[17] Y. Wang, B. Li, L. Zhang, P. Li, L. Wang, J. Zhang, Langmuir 28 (2011) 1657–1662.
[18] C.W. Lai, Y.H. Wang, C.H. Lai, M.J. Yang, C.Y. Chen, P.T. Chou, C.S. Chan, Y. Chi, Y.C. Chen, J.K. Hsiao, Small 4 (2008) 218–224.
[19] X. Peng, Y. Wang, X. Tang, W. Liu, Dyes Pigm. 91 (2011) 26–32.
[20] G. Trovati, E.A. Sanches, S.C. Neto, Y.P. Mascarenhas, G.O. Chierice, J. Appl. Polym. Sci. 115 (2009) 263–268.
[21] L. Jagannathan, R. Meenakshi, S. Gunasekaran, S. Srinivasan, Mol. Simulation 36 (2010) 283–290.
[22] G. Matrajt, J. Borg, P. Raynal, Z. Djouadi, L. d'Hendecourt, G. Flynn, D. Deboffle, Astron. Astrophys. 416 (2004) 983–990.
[23] F. Besson, R. Buchet, Spectrochim. Acta A 53 (1997) 1913–1923.
[24] W. Fathalla, M. Čajan, P. Pazdera, Molecules 5 (2000) 1210–1223.
[25] M. Unger, D. Chaturvedi, S. Mishra, P. Tandon, H.W. Siesler, Spectrosc. Lett. 46 (2013) 21–27.
[26] P. Musto, Macromolecules 36 (2003) 3210–3221.
[27] B. Bodenant, F. Fages, M.-H. Delville, J. Am. Chem. Soc. 120 (1998) 7511–7519.
[28] F.M. Winnik, Chem. Rev. 93 (1993) 587–614.
[29] S. Nishizawa, Y. Kato, N. Teramae, J. Am. Chem. Soc. 121 (1999) 9463–9464.
[30] D. Sahoo, V. Narayanaswami, C.M. Kay, R.O. Ryan, Biochemistry 39 (2000) 6594–6601.
[31] J.F. Callan, A.P de Silva, D.C. Magri, Tetrahedron 61 (2005) 8551–8588.
[32] S.R. Davidson, Adv. Phys. Org. Chem. 19 (1983) 1.
[33] T.K. Khan, M. Ravikanth, Dyes Pigm. 95 (2012) 89–95.
[34] H.J. Kim, J.E. Park, M.G. Choi, S. Ahn, S.-K. Chang, Dyes Pigm. 84 (2010) 54–58.
[35] S. Saha, P. Mahato, E. Suresh, A. Chakrabarty, M. Baidya, S.K. Ghosh, A. Das, Inorg. Chem. 51 (2011) 336–345.
[36] M.-H. Yang, P. Thirupathi, K.-H. Lee, Org. Lett. 13 (2011) 5028–5031.
[37] B. Liu, F. Zeng, S. Wu, J. Wang, F. Tang, Microchim. Acta (2013) 1–9.
[38] I.-T. Ho, T.-L. Lai, R.-T. Wu, M.-T. Tsai, C.-M. Wu, G.-H. Lee, W.-S. Chung, Analyst 137 (2012) 5770–5776.
[39] J. Isaad, Analyst 138 (2013) 3809–3819.
[40] P. Zarabadi-Poor, A. Badiei, A.A. Yousefi, J. Barroso-Flores, J. Mater. Chem. 117 (2013) 9281–9289.
[41] M. Vedamalai, S.-P. Wu, Org. Biomol. Chem. 10 (2012) 5410–5416.
[42] B. Liu, F. Zeng, G. Wu, S. Wu, Chem. Commun. 47 (2011) 8913–8915.
[43] M. Kumar, N. Kumar, V. Bhalla, H. Singh, P.R. Sharma, T. Kaur, Org. Lett. 13 (2011) 1422–1425.
[44] Y. Zhao, B. Zheng, J. Du, D. Xiao, L. Yang, Talanta 85 (2011) 2194–2201.